

Microchannel flow in the slip regime: gas-kinetic BGK–Burnett solutions

By KUN XU¹ AND ZHIHUI LI²

¹Mathematics Department, Hong Kong University of Science and Technology,
Clear Water Bay, Kowloon, Hong Kong
makxu@ust.hk

²China Aerodynamics Research and Development Centre, Mianyang 621000, PR China

(Received 28 April 2003 and in revised form 9 April 2004)

In the first part of this paper presents a gas-kinetic scheme based on the Bhatnagar–Gross–Krook (BGK) model for the microflow simulations in the near continuum flow regime. The current method improves the previous gas-kinetic BGK Navier–Stokes (BGK–NS) solver by (i) implementing a general non-equilibrium state based on the Chapman–Enskog expansion of the BGK model up to the Knudsen number squared (Kn)² in the gas distribution function, (ii) using the compatibility condition to evaluate all high-order time derivative terms in the Chapman–Enskog expansion, and (iii) implementing the kinetic boundary condition for the gas distribution function to obtain ‘slip’ boundary automatically. As a result, the gas-kinetic BGK–Burnett scheme improves the validity of the BGK–NS solver for the microchannel flow simulations even in the slip flow regime, where the Navier–Stokes equations with the slip boundary conditions are considered to be legitimately valid. Owing to the correction to the heat transport in the energy flux, the Prandtl number in the gas-kinetic BGK–Burnett method can take any value to capture both viscous and heat conduction effects. Since the current method is based on the direct evaluation of the gas distribution function and captures its time evolution, it is different from those methods that are based on the macroscopic Burnett or extended hydrodynamic equations. The second part of this paper is about the application of the newly developed gas-kinetic BGK–Burnett method in the microchannel flows. First, we verify the method in the pressure- and external-force-driven Poiseuille flows, where the reliable direct simulation Monte Carlo (DSMC) results are available. In the study of Poiseuille flow with $Kn = 0.1$, the qualitative differences in the pressure distribution in the cross-stream direction between the Navier–Stokes and the DSMC results are resolved by the gas-kinetic BGK–Burnett scheme. It demonstrates that the BGK–Burnett method could give a more realistic description of flow motion than the Navier–Stokes method even in the slip flow regime. After that, the current method is used to simulate the microchannel flows, where the experimental data are available. In this study, the similarity in the pressure distribution along the straight microchannel is verified first. Then, the mass flow rates for different gases, such as argon, helium and nitrogen, in the long microchannel of submicron height are computed and compared with the experimental measurements.

1. Introduction

Most microsystems involve fluid flows. When dealing with the flow in configurations of micrometres or less, many unexpected phenomena have been observed. The flows

in the macroscopic scale and microsystems are not quite the same. There is great demand to understand and develop numerical methods for the microflows. With the definition of Knudsen number Kn , which is the ratio between the mean free path and the characteristic length scale, such as the height of the microchannel, the flow in the microchannel is most probably in the slip $10^{-3} \leq Kn \leq 10^{-1}$ and transitional flow $10^{-1} \leq Kn \leq 10$ regimes. It is widely accepted that in the slip flow regime the continuum model, such as the Navier–Stokes equations with slip boundary condition, is still valid provided the velocity slip and temperature jump boundary conditions are used properly (Beskok & Karniadakis 1999). Based on the Navier–Stokes equations and the slip boundary condition, the analytical solutions for the flow distributions along the channel were obtained by many authors (i.e. Arkilic, Schmidt & Breuer 1997; Karniadakis & Beskok 2002; Zohar *et al.* 2002).

Direct simulations, for the microchannel flows in the slip regime, include mainly the direct simulation Monte Carlo (DSMC), the Boltzmann method, Navier–Stokes solvers and the methods based on the high-order moments equations. Even though the DSMC method is very successful in the high-speed rarefied gas regime (Bird 1994), its direct application to the near continuum regime has great numerical difficulties (Ho & Tai 1998; Oran, OH & Cybyk 1998). For example, how to control the statistical fluctuation and implementation of the inlet and outlet pressure boundary conditions becomes a challenge. For the DSMC method, a large sample size is often required to reduce the fluctuation to a level that is small in comparison with the macroscopic velocity, see Piekos & Breuer (1996) and Yan & Farouk (2002). The DSMC information preservation (DSMC-IP) method shows some promising results in this direction, see Fan & Shen (2001) and Cai *et al.* (2000). For the direct Boltzmann solver (Aristov 2001), the operator splitting techniques of separating the transport and collision processes numerically, may introduce large numerical dissipation in the near continuum regime when the time step used is much larger than the particle collision time, see Xu (2001) and Ohwada & Kobayashi (2004).

From the Boltzmann equation, the derivation of the Navier–Stokes equations through the Chapman–Enskog expansion is based largely on the assumption of local equilibrium and small gradients, which allow us to formulate the constitutive relations required to close the conservation equations. In situations where large gradients exist, such as in the strong shock layer, these assumption are expected to fail. Therefore, the validity of a macroscopic theory is theoretically restricted to situations in which the Knudsen number Kn is small. When the Kn number is not very small, i.e. $Kn > 0.001$, the slip boundary condition for the Navier–Stokes equations must be taken into account. However, there exist simple examples, as presented by Zheng, Garcia & Alder (2002*a,b*) and those in the current paper in §3, to show that even in the slip flow regime, the Navier–Stokes equations can give qualitatively different results from the reliable DSMC solutions. Therefore, in order to explore fully the flow physics in the slip regime, a scheme based on equations higher than the Navier–Stokes order becomes necessary. In other words, there is still room scientifically and practically to develop schemes beyond the Navier–Stokes equations in the slip flow regime for microflow simulations. In the past 70 years, many schemes have been developed for the Burnett equations. Agarwal, Yun & Balakrishnan (2001) presented an excellent review of the history of the Burnett equations. Owing to the complex nature of the Burnett orders, i.e. the connection between the material derivative and the spatial derivative or the stability considerations, many version of macroscopic Burnett equations have been adopted in the study of non-equilibrium

flow problems, such as the shock structure, boundary layer and the microchannel flows. However, for long microchannel flows, such as length of the order of thousands of micrometres, the direct simulation based on the Burnett equations has not yet been done.

In the past, gas-kinetic schemes have been developed successfully for the continuum flow simulations. The main idea of the gas-kinetic BGK-type schemes is first to translate the macroscopic flow variables into a gas distribution function, then the time evolution of the gas distribution function is followed based on the gas-kinetic model, such as the BGK model (Bhatnagar, Gross & Krook 1954), from which the flux is evaluated to update the macroscopic flow variables. Since the heat flux across the cell interface can be modified in the numerical scheme according to the correct Prandtl number, the validity of the BGK scheme is beyond the original BGK model with unit Prandtl number. In an early paper, the gas-kinetic BGK Navier–Stokes (BGK–NS) solver has been constructed and applied to many viscous and heat conduction flow problems (Xu 2001), such as the shock structure and boundary layer. Theoretically, as analysed by Ohwada (2002), the BGK–NS scheme is consistent with the railroad method derived from the gas-kinetic theory. In order to further increase the capacity of the BGK-type scheme in the near continuum flow simulation, in this paper we extend the BGK–NS method to the Burnett order, where higher-order terms in the Chapman–Enskog expansion are included in the gas distribution function. Since the gas-kinetic BGK–Burnett method follows the time evolution of the gas distribution function explicitly in the gas evolution stage, it is different from any other approach where the macroscopic Burnett equations are discretized directly, such as the method of Balakrishnan (1999). In the current gas-kinetic method, because all flow variables are simply the moments of a single particle distribution function, numerically it becomes more convenient to follow a single distribution function rather than all higher-order terms in the Burnett equations. For example, in the gas-kinetic scheme, the higher-order temporal variations in the gas distribution function can be evaluated directly according to the compatibility condition. Furthermore, since the gas distribution function is evaluated explicitly at the boundary, the reflection of the particles can be done easily. This is one of the advantages of using the gas-kinetic BGK–Burnett method in the microchannel flow rather than discretizing the macroscopic Burnett equations directly.

After constructing the numerical scheme, we use it in the study of microchannel flow. First, it is used in the external-force- and pressure-driven Poiseuille flow in the slip flow regime with $Kn=0.1$. In the early studies by Zheng *et al.* (2002*a,b*), the qualitative differences in the results between the Navier–Stokes with slip boundary condition and the DSMC are realized. The BGK–Burnett calculation in this paper confirms the accuracy of the DSMC solution and points out the necessity of developing a higher-order method, even in the slip flow regime. As the Knudsen number increases, such as in the regime $0.1 \leq Kn \leq 1.0$, the difference between the BGK–Burnett and BGK–NS solutions in the mass flow rate can be clearly seen in figure 8. Following the validation of the BGK–Burnett method, it is then applied to the microchannel flow calculations. Owing to the significant scatter of the experimental data, the most recent and accurate experiments of Zohar *et al.* (2002) are tested. The simulation results are compared with the experimental data for different gases under different flow conditions. Also, the similarity and differences between the gas-kinetic BGK–Burnett solution and the analytic solution of the Navier–Stokes equations of Arkilic *et al.* (1997) are presented.

2. A gas-kinetic BGK–Burnett flow solver

The focus in a finite-volume gas-kinetic scheme is to construct a time-dependent gas distribution function f at a cell interface, from which the numerical flux can be obtained. For example, in the one-dimensional case, the Navier–Stokes or Burnett equations can always be written in a conservative form, $W_t + F_x = 0$, where W is the conservative flow variable and F is the corresponding flux. Numerically, this equation can be discretized as

$$W_j^{n+1} = W_j^n + \frac{1}{\Delta x} \int_{t^n}^{t^{n+1}} (F_{j-1/2}(t) - F_{j+1/2}(t)) dt,$$

where Δx is the cell size and $\Delta t = t^{n+1} - t^n$ is the time step. The gas-kinetic scheme is mainly about the evaluation of the fluxes at the cell interface in the above equation.

2.1. Initial macroscopic data reconstruction

For the Navier–Stokes equations, the stress and heat conduction terms are proportional to the first-order derivatives of macroscopic variables. So, in the BGK–NS scheme (Xu 2001), based on the cell averaged initial macroscopic variables, only the piecewise linear flow distributions inside each cell are constructed, such as the density distribution $\rho = \rho_0 + \rho_1 x$. In order to extend the BGK scheme to the Burnett order, a second-order interpolation for the macroscopic flow variables is required, from which a non-equilibrium gas distribution function up to $(Kn)^2$ can be obtained.

Suppose at the beginning of each time step t^n , the cell averaged mass, momentum and energy for a two-dimensional flow are denoted by $w_j = (\rho_j, (\rho U)_j, (\rho V)_j, (\rho E)_j)$ in the cell j for $x \in [x_{j-1/2}, x_{j+1/2}]$ with cell size Δx . The interface $x_{j+1/2}$ between cells j and $j + 1$ is assumed to be $x_{j+1/2} = 0$. With the initial data $w_{j-1}, w_j, w_{j+1}, w_{j+2}$, the continuous flow distribution around $x = 0$ can be constructed as

$$\bar{w}(x, 0) = w_0 + w_1 x + \frac{1}{2} w_2 x^2, \quad (1)$$

where up to the third-order accuracy, the cell interface values and their first- and second-order spatial derivatives have the form

$$w_0 = [7(w_j + w_{j+1}) - (w_{j-1} + w_{j+2})]/12,$$

$$w_1 = [5(w_{j+1} - w_j)/4 - (w_{j+2} - w_{j-1})/12]/\Delta x,$$

and

$$w_2 = 3(w_j + w_{j+1} - 2w_0)/(\Delta x)^2.$$

Note that w_0, w_1 and w_2 all have four components to represent the mass, x and y momentum, and energy distribution.

2.2. Gas-kinetic BGK–Burnett method

In this subsection, a directional splitting method to solve the two-dimensional BGK equation will be presented. The BGK model in the x -direction can be written as (Bhatnagar *et al.* 1954)

$$f_t + u f_x = \frac{g - f}{\tau}, \quad (2)$$

where f is the gas distribution function and g is the equilibrium state approached by f . Both f and g are functions of space x , time t , particle velocities (u, v) and internal variable ξ . The particle collision time τ is related to the viscosity and heat

conduction coefficients. The equilibrium state is a Maxwellian distribution,

$$g = \rho \left(\frac{\lambda}{\pi} \right)^{(K+2)/2} \exp(-\lambda((u-U)^2 + (v-V)^2 + \xi^2)),$$

where ρ is the density, U and V are the macroscopic velocities in the x - and y -directions, and $\lambda = m/2kT$, where m is the molecular mass, k is the Boltzmann constant, and T is the temperature. For a two-dimensional flow with an explicit account of macroscopic U and V velocities, the random particle motion in the z -direction is included in the internal variable ξ , and the total number of degrees of freedom K in ξ is

$$K = \frac{2}{\gamma - 1} - D, \quad (3)$$

where D is the dimension of the space. For example, for a monatomic gas with $\gamma = 5/3$, K is equal to 1 to account for the particle motion in the z -direction. For a diatomic gas with $\gamma = 1.4$, besides the random z -direction motion, there are also two internal rotating degrees of freedom. Therefore, $K = 3$ for a diatomic gas. The internal variable $\xi^2 = \xi_1^2 + \xi_2^2 + \dots + \xi_K^2$. The relation between mass ρ , momentum ($\rho U, \rho V$), and energy ρE densities with the distribution function f is

$$\begin{pmatrix} \rho \\ \rho U \\ \rho V \\ \rho E \end{pmatrix} = \int \psi_\alpha f \, d\mathcal{E} \quad (\alpha = 1, 2, 3, 4), \quad (4)$$

where ψ_α is the component of the vector of moments

$$\boldsymbol{\psi} = (\psi_1, \psi_2, \psi_3, \psi_4)^T = (1, u, v, \frac{1}{2}(u^2 + v^2 + \xi^2))^T,$$

and $d\mathcal{E} = du \, dv \, d\xi$ is the volume element in the phase space with $d\xi = d\xi_1 \, d\xi_2 \dots d\xi_K$. Since mass, momentum and energy are conserved during particle collisions, f and g satisfy the conservation constraint,

$$\int (g - f) \psi_\alpha \, d\mathcal{E} = 0 \quad (\alpha = 1, 2, 3, 4), \quad (5)$$

at any point in space and time.

With the consideration of different time and length scales in the transport and collision operators of the Boltzmann equation, the BGK model can also be written in a dimensionless form

$$Kn(\tilde{f}_{\tilde{t}} + \tilde{u} \tilde{f}_{\tilde{x}}) = (\tilde{g} - \tilde{f})/\tilde{\tau},$$

where Kn is the local Knudsen number. With the expansion of the solution \tilde{f} ,

$$\tilde{f} = \tilde{g} + Kn \tilde{f}_1 + Kn^2 \tilde{f}_2 + \dots, \quad (6)$$

the Chapman–Enskog expansion can be used successively to determine all function forms of $\tilde{f}_1, \tilde{f}_2, \dots$. Up to the Burnett order, only \tilde{f}_2 is required. Besides the standard Chapman–Enskog expansion, we can also find the solution of the BGK model (2) directly by using the iterative method. For example, up to the Burnett order, the iterative method for the BGK equation (2) gives the solution,

$$f = g - \tau Dg + \tau D(\tau Dg), \quad (7)$$

where $D = \partial_t + u \partial_x$ and u is the particle velocity. It can be shown that up to the super-Burnett order, the formal Chapman–Enskog solution (6) and the iterative

solutions (7) are identical, see Ohwada & Xu (2003). Since we are going to develop a scheme for the local time evolution around a cell interface, the variations of collision time τ around a cell interface within a time step are ignored. Therefore, (7) can be simplified,

$$f = g - \tau Dg + \tau^2 D^2 g. \quad (8)$$

Note that spatial and temporal variation of τ at different numerical cells and different time steps are still accounted for in the current BGK–Burnett scheme by changing τ cell by cell according to the viscosity coefficient and local pressure, equation (15).

The macroscopic BGK–Burnett equations of Balakrishnan (1999) are derived from the simplified iterative solution. Since the compatibility condition $\int \psi D^2 g d\mathcal{E} = 0$ cannot be satisfied simply in their approach, Balakrishnan designed additional moment closure terms in f_2 in the derivation of macroscopic BGK–Burnett equations. Also, with more realistic considerations, such as the variation of the collision frequency, the macroscopic BGK–Burnett equations have been subsequently modified in past years, such as the versions of 1996, 1998 and 1999 in Balakrishnan (1999). The current gas-kinetic BGK–Burnett method is different from the previous approaches mainly in the following respects. (i) The gas-kinetic BGK–Burnett scheme is based on the evaluation of the gas distribution function directly without discretizing the macroscopic Burnett equations, even without knowing the explicit forms of the Burnett equations. (ii) The construction of the time-dependent gas distribution function f up to τ^2 terms involves second-order temporal derivatives of a Maxwellian distribution. Different from Balakrishnan’s closure method, the unknowns related to g_{tt} in the current method (see below) are uniquely evaluated according to the compatibility condition $\int \psi f_2 d\mathcal{E} = 0$. (iii) As shown below, the current BGK–Burnett method can justify the Prandtl number according to the values of the real gases. Therefore, both viscous and heat conduction effects can be captured. (iv) Owing to the evaluation of the gas distribution function, the slip boundary condition can be obtained automatically with the particle reflections from the boundary.

The general solution f of the BGK model (2) at a cell interface $x_{i+1/2,j}$ and time t is

$$f(x_{i+1/2,j}, t, u, v, \xi) = \frac{1}{\tau} \int_0^t g(x', t', u, v, \xi) e^{-(t-t')/\tau} dt' + e^{-t/\tau} f_0(x_{i+1/2,j} - ut), \quad (9)$$

where $x' = x_{i+1/2,j} - u(t - t')$ is the particle trajectory and f_0 is the initial gas distribution function f at the beginning of each time step ($t = 0$). Two unknowns g and f_0 must be specified in (9) in order to obtain the solution f . In order to simplify the notation, $x_{i+1/2,j} = 0$ will be used in the following text.

In order to obtain the solution f in (9), we must first evaluate the initial non-equilibrium state f_0 at the beginning of each time step. For the microflows, the thickness of the channel may be of the order of the mean free path. If the flow structure inside the channel is well resolved by the mesh size, such as 20 grid points in the vertical direction of the channel, different from the shock capturing scheme, there is no need to introduce flow discontinuities at the cell interface to include the additional kinematic dissipation in the initial data (Xu 2001). So, in the smooth-flow case, up to the Burnett order, the non-equilibrium distribution function at $t = 0$ has the form,

$$f_0(x, 0) = g(x, 0) - \tau Dg + \tau^2 D^2 g,$$

where g is the equilibrium state, and $-\tau Dg$ and $\tau^2 D^2 g$ contribute the non-equilibrium parts corresponding to the Navier–Stokes and Burnett orders (Ohwada & Xu 2003).

More specifically, the non-equilibrium distribution f_1 for the Navier–Stokes order has the form

$$f_1 = -\tau Dg = -\tau(g_t + ug_x),$$

and for the Burnett order

$$f_2 = \tau^2(D^2g + B''g) = \tau^2(g_{tt} + 2ug_{xt} + u^2g_{xx} + B''g),$$

where B'' is from the time derivative of a certain part in τDg , which will be given explicitly later. Therefore, the initial non-equilibrium states can be written as

$$f_0(x, 0) = g(x, 0) - \tau(g_t + ug_x) + \tau^2(g_{tt} + 2ug_{xt} + u^2g_{xx} + B''g).$$

When we further expand $g(x, 0)$, $g_t(x, 0)$ and $g_x(x, 0)$ around the point $(x = 0, t = 0)$, up to the second-order spatial derivatives we have

$$f_0(x, 0) = g(0, 0) + g_x x + \frac{1}{2}g_{xx}x^2 - \tau(g_t + ug_x) - \tau(g_{xt} + ug_{xx})x + \tau^2(g_{tt} + 2ug_{xt} + u^2g_{xx} + B''g).$$

The direct Taylor expansions of a Maxwellian distribution function g can be expressed as

$$\begin{aligned} g_x &= ag, & g_t &= Ag, \\ g_{xx} &= (a^2 + b)g, & g_{xt} &= (aA + C)g, \\ g_{tt} &= (A^2 + B')g, \end{aligned}$$

where all parameters a, A, b, C, B' and B'' have the following functional dependences on ψ ,

$$q = q_1 + q_2u + q_3v + q_4(u^2 + v^2 + \xi^2).$$

In other words, there are four unknowns in each of the parameters (a, A, b, B', B'', C) in the two-dimensional case. With the above definitions, the initial non-equilibrium state around a cell interface becomes

$$\begin{aligned} f_0(x, 0) &= (1 + ax + \frac{1}{2}(a^2 + b)x^2)g(0, 0) \\ &\quad - \tau[(ua + A) + ((aA + C) + u(a^2 + b))x]g(0, 0) \\ &\quad + \tau^2[(A^2 + B) + 2u(aA + C) + u^2(a^2 + b)]g(0, 0), \end{aligned} \quad (10)$$

where $B = B' + B''$. From the initially interpolated macroscopic variables in (1), we can determine f_0 through the connection between macroscopic and microscopic variables,

$$w_0 + w_1x + \frac{1}{2}w_2x^2 = \int f_0\psi_\alpha d\mathcal{E} \quad (\alpha = 1, 2, 3, 4).$$

In order to further simplify the notation, let us define $\langle \cdots \rangle$ as

$$\langle \cdots \rangle = \int (\cdots)\psi_\alpha g(0, 0) d\mathcal{E} \quad \text{for } \alpha = 1, 2, 3, 4.$$

Then, the equilibrium state $g(0, 0)$ can be determined first by

$$w_0 = \int \psi_\alpha g(0, 0) d\mathcal{E} = \langle 1 \rangle.$$

For example, the free parameters $(\rho_0, U_0, V_0, \lambda_0)$ in $g(0, 0)$ can be found from

$w_0 = (\rho_0, \rho_0 U_0, \rho_0 V_0, \rho_0 E_0)^T$, such as

$$\lambda_0 = \frac{K+2}{4} \frac{\rho_0}{\rho_0 E_0 - \frac{1}{2}\rho_0(U_0^2 + V_0^2)}.$$

Consequently, the parameters a_1, a_2, a_3 and a_4 in $a = a_1 + a_2 u + a_3 v + a_4(u^2 + v^2 + \xi^2)$ and b_1, b_2, b_3 and b_4 in $b = b_1 + b_2 u + b_3 v + b_4(u^2 + v^2 + \xi^2)$ can be found from

$$\langle a \rangle = w_1 \equiv \left(\frac{\partial \rho}{\partial x}, \frac{\partial(\rho U)}{\partial x}, \frac{\partial(\rho V)}{\partial x}, \frac{\partial(\rho E)}{\partial x} \right)^T,$$

$$\langle (a^2 + b) \rangle = w_2 \equiv \left(\frac{\partial^2 \rho}{\partial x^2}, \frac{\partial^2(\rho U)}{\partial x^2}, \frac{\partial^2(\rho V)}{\partial x^2}, \frac{\partial^2(\rho E)}{\partial x^2} \right)^T.$$

For detailed formulation about the evaluation of all parameters in a and b from the above equations, see the Appendix in Xu (2001).

After finding a and b , based on the condition on the Chapman–Enskog expansion, such as $\langle f_1 \rangle = 0$ and $\langle f_2 \rangle = 0$, we have

$$\left. \begin{aligned} \langle A + ua \rangle &= 0, \\ \langle C + aA + u(a^2 + b) \rangle &= 0, \\ \langle B' + A^2 + u(Aa + C) \rangle &= 0, \end{aligned} \right\} \quad (11)$$

and

$$\langle B + A^2 + 2u(aA + C) + u^2(a^2 + b) \rangle = 0. \quad (12)$$

Therefore, the parameters A, C, B' and B'' are uniquely obtained from the above equations. The use of (11) and (12) not only uniquely determines all coefficients in A and B , but also satisfies the compatibility condition $\int \psi f_1 d\mathcal{E} = 0$ and $\int \psi f_2 d\mathcal{E} = 0$. It can be shown that under the assumption of local constant τ , the above iterative solution is identical to the formal solution in the Chapman–Enskog expansion of the BGK model (Ohwada & Xu 2003). In other words, the above expansion for the BGK Burnett solution is unique and there is no freedom to change any parameter.

After having f_0 at the beginning of each time step, in a well-resolved microchannel flow, we can expand the equilibrium state $g(x, t)$ around $(x = 0, t = 0)$ as well,

$$g(x, t) = [1 + ax + \frac{1}{2}(a^2 + b)x^2 + At + \frac{1}{2}(A^2 + B')t^2 + (C + Aa)xt]g(0, 0). \quad (13)$$

When substituting both f_0 and g into the integral solution of the BGK model (9), we have

$$f(0, t) = g \left[1 - \tau au + (-\tau + t)A + (\tau^2 - \tau t + \frac{1}{2}t^2)(A^2 + B') \right. \\ \left. + (2\tau^2 - \tau t)(aA + C)u + \tau^2(a^2 + b)u^2 + B''(\tau^2 - \tau t) \right]. \quad (14)$$

This is the time accurate gas distribution function at a cell interface for the flux evaluation in the gas-kinetic BGK–Burnett scheme. If f only keeps the first few terms, such as

$$f = g[1 - \tau au + (-\tau + t)A],$$

in the smooth flow region the BGK–NS scheme is recovered (see Xu 2001).

In the above particle distribution function, the only unknown is the particle collision time τ . From the gas-kinetic theory (Vincenti & Kruger 1965), the dynamic viscosity coefficient μ can be expressed as,

$$\mu = \tau p, \quad (15)$$

where τ is the particle collision time and p is local pressure. The viscosity coefficient μ can be evaluated according to the molecular model of particle interaction, such as the hard-sphere or soft-sphere models, or given by the experiments. Therefore, τ is determined locally from (15). For example, up to the Navier–Stokes order $f = g - \tau Dg$, the viscous stress for the BGK model is

$$\sigma_{kl} = \tau p \left[\left(\frac{\partial U_k}{\partial x_l} + \frac{\partial U_l}{\partial x_k} - \frac{2}{3} \delta_{kl} \frac{\partial U_i}{\partial x_i} \right) + \frac{2\mathcal{K}}{3(\mathcal{K} + 3)} \delta_{kl} \frac{\partial U_i}{\partial x_i} \right], \quad (16)$$

where \mathcal{K} is the rotational degree of freedom (equation (3)), such as $\mathcal{K} = 2$ for a diatomic gas. As noted in (16), the corresponding first and second viscosity coefficients are

$$\mu = \tau p, \quad \zeta = \mu \frac{2\mathcal{K}}{3(\mathcal{K} + 3)}. \quad (17)$$

For a monatomic gas, the bulk viscosity $\zeta = 0$. For a diatomic gas, $\zeta = 4/15\mu$. Since the compressibility for the microchannel flow is small, the bulk viscosity term has a limited effect on the macroscopic flow distribution.

With the gas distribution function in (14), the time-dependent numerical fluxes in the gas-kinetic BGK–Burnett solver in the x -direction across the cell interface are computed by

$$\begin{pmatrix} \mathcal{F}_{\rho} \\ \mathcal{F}_{\rho U} \\ \mathcal{F}_{\rho V} \\ \mathcal{F}_{\rho E} \end{pmatrix}_{i+1/2,j} = \int u \begin{pmatrix} 1 \\ u \\ v \\ \frac{1}{2}(u^2 + v^2 + \xi^2) \end{pmatrix} f(x_{i+1/2,j}, t, u, v, \xi) d\mathcal{E}. \quad (18)$$

By integrating (18) to the whole time step Δt , we obtain the total mass, momentum and energy transport. Similarly, the flux $\mathcal{G}_{i,j+1/2}$ in the y -direction can be evaluated as well. Therefore, the flow variables of mass, momentum and energy densities $W = (\rho, \rho U, \rho V, \rho E)^t$ inside each cell can be updated by

$$W_{i,j}^{n+1} = W_{i,j}^n + \frac{1}{\Delta x} \int_0^{\Delta t} (\mathcal{F}_{i-1/2,j} - \mathcal{F}_{i+1/2,j}) dt + \frac{1}{\Delta y} \int_0^{\Delta t} (\mathcal{G}_{i,j-1/2} - \mathcal{G}_{i,j+1/2}) dt.$$

In the external force driven flow, additional force terms in the momentum and energy equations must be added on the right-hand side of the above equation. Since the gas-kinetic BGK–Burnett method is an explicit time accurate scheme, the time steps Δt in all calculations are determined by CFL and the stability condition from the dissipative term $\Delta t \simeq (\Delta x)^2/2\nu$, where ν is the kinematic viscosity coefficient $\nu = \mu/\rho$. All steady-state solutions are obtained from the time accurate BGK–Burnett solver with long time integration.

2.3. Prandtl number fix in the gas-kinetic BGK–Burnett scheme

It is well known that the above BGK–Burnett scheme corresponds to unit Prandtl number. In order to simulate the flow with any realistic heat conduction coefficient, we have to modify the above formulation. Similar to the Shakhov (1968) model, the simplest way to do this is to adjust the heat flux in the total energy flux of (18) (Chae, Kim & Rho 2000; Xu 2001). Since f at the cell interface is explicitly evaluated in (14), the time-dependent heat flux can be obtained precisely,

$$q = \frac{1}{2} \int (u - U)((u - U)^2 + (v - V)^2 + \xi^2) f d\mathcal{E}, \quad (19)$$

where the average velocities U and V are defined by

$$U = \int uf \, d\mathcal{E} \Big/ \int f \, d\mathcal{E}, \quad V = \int vf \, d\mathcal{E} \Big/ \int f \, d\mathcal{E}.$$

Then, after evaluating the heat flux q , for a specific Prandtl number Pr , such as $Pr = 2/3$ for the monatomic gas and $Pr = 0.72$ for the diatomic gas, we can modify the total energy flux (18) as

$$\mathcal{F}_{\rho E}^{new} = \mathcal{F}_{\rho E} + \left(\frac{1}{Pr} - 1 \right) q. \quad (20)$$

Little computational time is involved in the above Prandtl number fix, since all momentum in q has been obtained in the evaluation of the original energy flux. In other words, the reliability of the above gas-kinetic BGK–Burnett method is beyond the BGK model itself. It can be considered as a new discretized model in the near continuum flow regime. We emphasize again that the gas-kinetic BGK–Burnett scheme is based on the direct evaluation of the gas distribution function at a cell interface (14) rather than discretizing the macroscopic Burnett equations.

2.4. Gas-kinetic boundary condition

The interaction between the gas flow and the solid boundary has been explicitly pointed out by many authors (see Patterson 1956; Cercignani 2000). This section is mainly about how to implement these ideas numerically in the gas-kinetic BGK–Burnett scheme.

For the microflows in the near continuum regime, even for the Navier–Stokes equations the application of the slip boundary condition becomes necessary. Since the gas-kinetic BGK schemes are based on the time evolution of gas distribution function to update the flow variables, the slip boundary condition can be obtained naturally for both the BGK–NS and BGK–Burnett methods.

In the slip flow regime, with the one-sided interpolation of the conservative variables up to the wall, we can use the technique presented in the last section to evaluate the gas distribution function f^{in} there, see (14). Therefore, we can evaluate the total number of particles hitting the wall $\int_0^{\Delta t} \int_{u<0} uf^{in} \, d\mathcal{E} \, dt$. All these particles will be reflected from the wall according to the specular reflection coefficient β . With the assumption of wall temperature λ_w , we can construct an equilibrium state there first, i.e.

$$g^w = \rho_w \left(\frac{\lambda_w}{\pi} \right)^{(K+2)/2} \exp(-\lambda_w(u^2 + v^2 + \xi^2)).$$

In the above equilibrium state, the solid wall is assumed to be stationary. The requirement that no particles penetrate the wall is equivalent to

$$\int_0^{\Delta t} \int_{u>0} g^w \, d\mathcal{E} \, dt = - \int_0^{\Delta t} \int_{u<0} uf^{in} \, d\mathcal{E} \, dt,$$

from which the density ρ_w in g^w can be obtained

$$\rho_w = - \frac{2\sqrt{\pi\lambda_w}}{\Delta t} \int_0^{\Delta t} \int_{u<0} uf^{in} \, d\mathcal{E} \, dt.$$

Therefore, the total gas distribution function at the wall for the accommodation coefficient ($\sigma = 1 - \beta$) can be written as

$$f^{total} = (1 - \beta)g_{u>0}^w + f_{u<0}^{in} + \beta f_{u<0}^{in}(-u, v),$$

where the term $\beta f_{u<0}^{in}(-u, v)$ accounts for the component with specular reflection from the surface. In the case of no specular reflection, such as the full accommodation case $\sigma = 1$, β is equal to 0. In all our calculations in this paper, $\sigma = 1$ is used. After obtaining the gas distribution function f^{total} at the wall, the flux across the solid boundary can be evaluated in the same way as (18). The slip boundary condition forms automatically from f^{total} in the gas-kinetic BGK scheme, such as the slip velocity

$$V_{slip} = \frac{\int v f^{total} d\mathcal{E}}{\int f^{total} d\mathcal{E}} \neq 0,$$

along the solid surface.

Inlet and outlet boundary conditions for the pressure-driven microchannel flows are the following. At both inlet and outlet faces, the pressure, temperature and transverse flow velocity are specified at the inlet, leaving the streamwise velocity to be obtained using second-order interpolation from the interior region, the inflow boundary conditions are imposed as

$$\rho_{in} = \rho_+, \quad p_{in} = p_+, \quad U_{in} = 2U_1 - U_2, \quad V_{in} = 0,$$

where 1 refers to the first cell inside the computational domain, 2 is the second cell, and p_+ and ρ_+ are the given inlet pressure and density while the temperature for the incoming gas is known in experiments. For the outflow boundary condition, only the pressure is specified and the remaining variables are obtained by the second-order extrapolation from interior region. The outflow boundary conditions are

$$\rho_{out} = 2\rho_{out-1} - \rho_{out-2}, \quad p_{out} = p_-, \quad U_{out} = 2U_{out-1} - U_{out-2}, \quad V_{out} = 2V_{out-1} - V_{out-2}$$

where $(out - 1)$ is the last cell inside the computational domain, and p_- is the given outlet pressure. The implementation of similar kinetic boundary condition is also discussed for the discrete particle velocity method in Li & Zhang (2004).

3. Study of microchannel flows

In this section, the gas-kinetic BGK–Burnett scheme developed in the last section will be used to study the microchannel flows in the slip flow regime. The cases studied include the Poiseuille flow and the experiments of Zohar *et al.* (2002).

3.1. External force and pressure driven Poiseuille flows

The first case is about Poiseuille flow under the external forcing term with the Knudsen number $Kn = 0.1$. As pointed out by many authors, see Santos *et al.* (1989), Malek, Baras & Garcia (1997), Uribe & Garcia (1999) and Aoki, Takata & Nakanishi (2002), even for this simple case with relative small gradient and Knudsen number, the Navier–Stokes equations fail to predict a qualitative correct solution. Specifically, for the external-force-driven case, the Navier–Stokes equations fail to reproduce the central minimum in the temperature profile and a non-constant pressure profiles in the cross-stream direction, which are both predicted by the kinetic theory and observed in the DSMC simulations. Furthermore, based on the

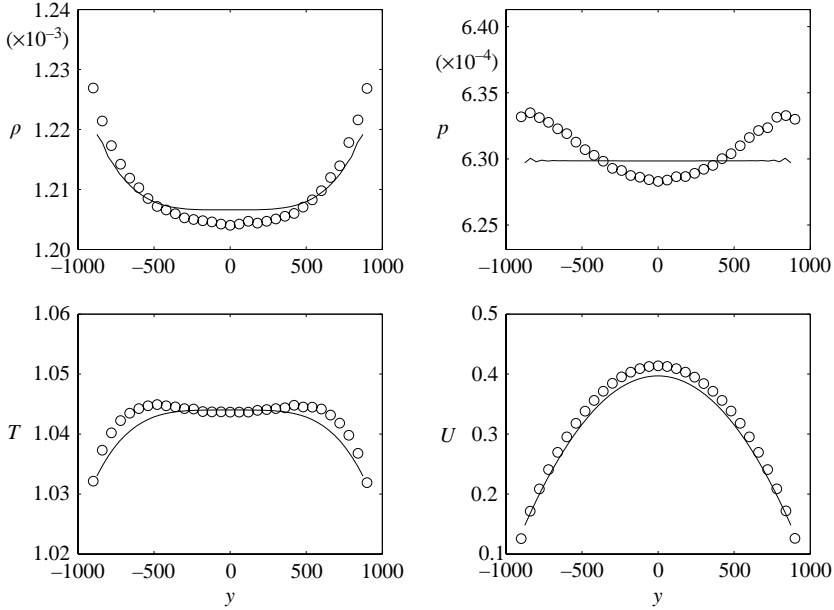


FIGURE 1. Flow distribution in the cross-stream direction in the external-force-driven case. \circ , DSMC results (Zheng *et al.* 2002b); —, BGK-NS solutions (Xu 2001). The constant pressure distribution in the Navier-Stokes solution is independent of the slip boundary conditions.

Navier-Stokes equations, it is not possible to correct this failure by modifying the equation of state, transport coefficients or boundary conditions. Unlike the slip phenomena, the discrepancy is not just near a boundary, but throughout the system. The similar discrepancy is also happening for the pressure-driven case.

The set-up of the external force driven case is as follows (Zheng *et al.* 2002a, b). The simulation fluid is a hard sphere gas with reference particle mass $m = 1$ and diameter $d = 1$. At the reference density of $\rho_0 = 1.21 \times 10^{-3}$, the mean free path is $l_0 = m/(\sqrt{2}\pi\rho_0 d^2) = 186$. The distance between the thermal walls is $L_y = 10l_0$ and their temperature is set at $T_0 = 1.0$. The reference fluid speed is $U_0 = 1 = \sqrt{2kT_0/m}$, so the Boltzmann constant is taken as $k = 1/2$. The reference sound speed is $c_0 = \sqrt{\gamma kT_0/m} = 0.91$ with $\gamma = 5/3$ for a monatomic gas. The reference pressure is $p_0 = \rho_0 kT_0/m = 6.05 \times 10^{-4}$. The acceleration and pressure gradient are chosen so that the flow will be subsonic, laminar and of similar magnitude in the two cases. Specifically, $\rho_0|\mathbf{f}| = 8.31 \times 10^{-8}$ for the acceleration-driven case and $dp/dx = 1.08 \times 10^{-7}$ for the pressure-driven case ($p_+ = 3p_0/2$, $p_- = p_0/2$, $L_x = 30l_0$), in both cases the Knudsen number is $Kn = l_0/L_y = 0.1$ and the Reynolds number is of order one. In all calculations, the cell size is half the mean free path of the initial data.

Figure 1 presents the results for the force-driven case in the cross-stream direction using the BGK-NS method (Xu 2001) with the slip kinetic boundary condition presented in the last section. The circles in figure 1 are the well-verified DSMC results (Zheng *et al.* 2002b). Since the BGK-NS is an accurate Navier-Stokes solver, even with the slip boundary condition, the pressure distribution is a constant in the cross-stream direction, which is different from the DSMC solution. In the paper by Zheng *et al.* (2002b), a different Navier-Stokes solver is used for the NS solution, but

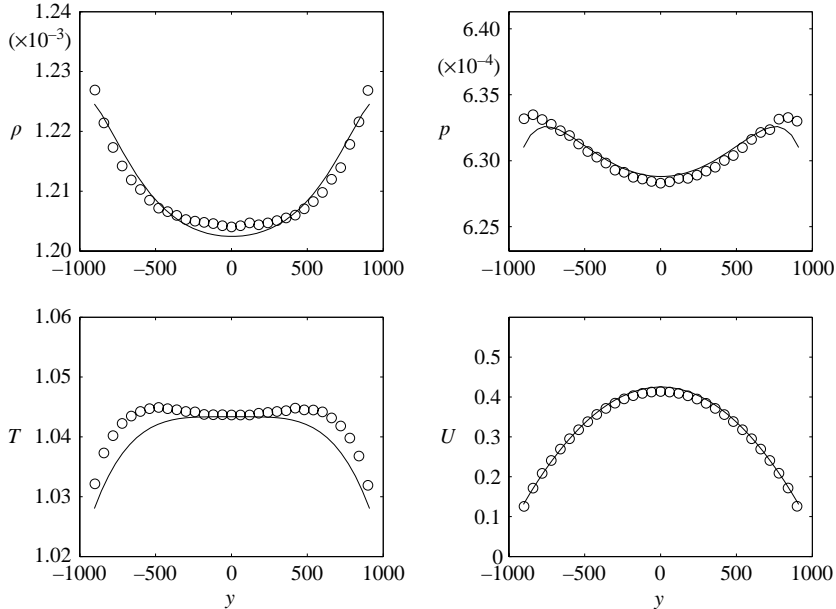


FIGURE 2. Flow distribution in the cross-stream direction in the external-force-driven case. \circ , DSMC results (Zheng *et al.* 2002b); —, gas-kinetic BGK Burnett.

both NS methods give similar results qualitatively. In order to resolve the discrepancy between the NS and DSMC solutions, the gas-kinetic BGK–Burnett solver developed in the last section is used and figure 2 is the simulation result. As shown in this figure, the curved pressure distribution in the cross-stream direction is captured well. So, up to the Burnett order, the non-constant pressure distribution can be obtained. This result is consistent with the analysis in Uribe & Garcia (1999); however, the temperature minimum at the centre does not appear in the current BGK–Burnett solution. The temperature minimum at the centre can be explained using the gas-kinetic BGK–super-Burnett scheme (Xu 2003).

For the pressure driven case, the length of the channel is about 30 mean free paths. First, the BGK–NS code is used in this case as well. Figure 3 shows the flow distribution along the centreline of the channel, where the circles are the DSMC solutions. As seen in this figure, the BGK–NS code does capture the flow distribution accurately in the stream direction, which is consistent with the general belief that the Navier–Stokes equations with the slip boundary condition can be faithfully applied in the slip flow regime of $Kn \leq 0.1$ (Karniadakis & Beskok 2002). However, in the cross-stream direction at the middle of the channel, the flow distribution calculated by the BGK–NS code is shown in figure 4. This figure clearly shows the inconsistency in pressure distribution between the BGK–NS and DSMC solutions. For example, the Navier–Stokes equations with slip boundary condition predict the maximum pressure at the centre. However, the DSMC gives the opposite conclusion. This phenomenon is irrelevant with the slip boundary condition or constitutive relationship. This phenomena clearly shows that a scheme based on equations higher than the Navier–Stokes is necessary to explore the flow behaviour in the slip regime. Figure 5 is the result from the current BGK–Burnett scheme. Except for the small variation along the boundary, there is excellent agreement in the interior region between the DSMC and the BGK–Burnett solutions. In other words, the correct

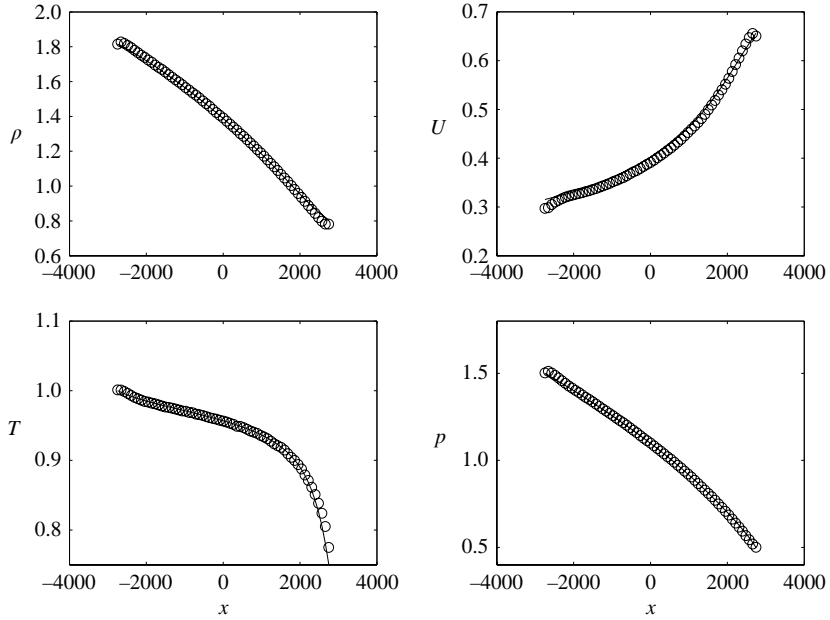


FIGURE 3. Flow distribution in the stream direction in the pressure-driven case. \circ , DSMC results (Zheng *et al.* 2002b); —, BGK-NS solutions (Xu 2001). In the stream direction, the Navier-Stokes equations plus slip boundary condition give accurate solutions.

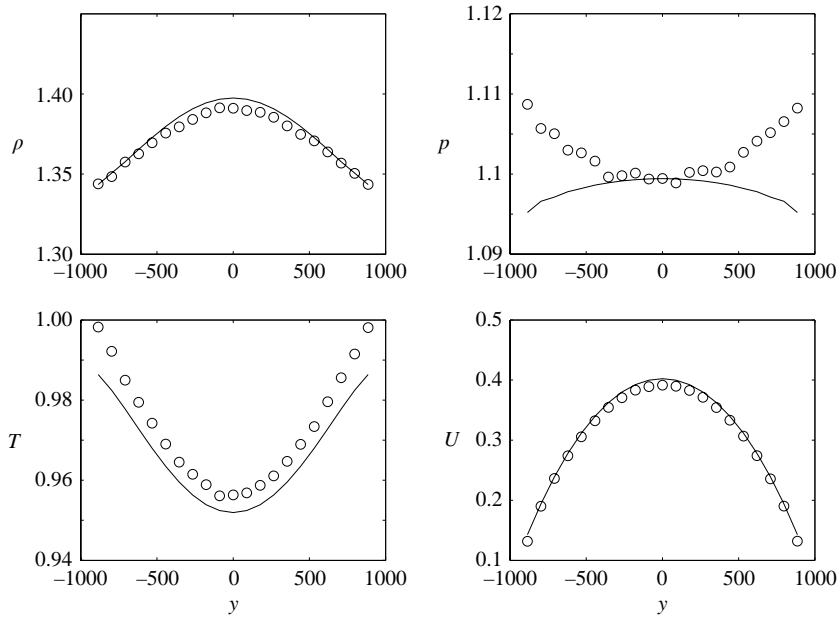


FIGURE 4. Flow distribution in the cross-stream direction in the pressure-driven case. \circ , DSMC results (Zheng *et al.* 2002b); —, BGK-NS solutions (Xu 2001). The Navier-Stokes equations give the opposite curve to the DSMC in the pressure distribution.

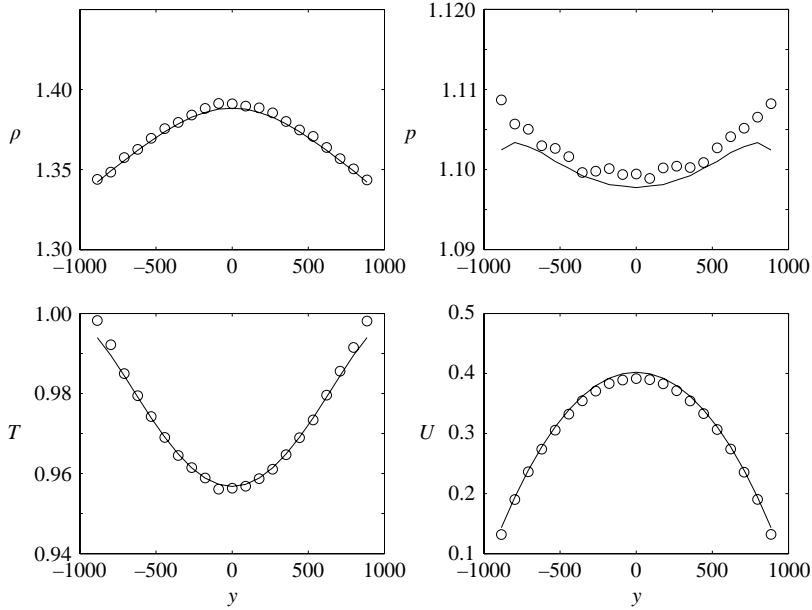


FIGURE 5. Flow distribution in the cross-stream direction in the pressure-driven case. \circ , DSMC results (Zheng *et al.* 2002b); —, BGK–Burnett solutions. The curved pressure distribution is captured in the BGK–Burnett solution.

capturing of the pressure distribution in the cross-stream direction is beyond the Navier–Stokes equations. In terms of efficiency, the BGK–Burnett is much faster than the DSMC code. For the current calculation in the pressure-driven case, the BGK–Burnett uses less than half an hour to obtain the converged flow distribution using a standard PC with Pentium IV processor. However, it takes days for the DSMC method to reduce the statistical noise and obtain a smooth solution. Figures 6 and 7 show the two-dimensional contours of the BGK–Burnett (upper) and the DSMC (lower) solutions for the pressure-driven case. Since the V velocity in the cross-stream direction is very small in comparison with the U velocity, as shown in figure 7, it is hard for the DSMC method to capture such a small value. To obtain a smooth inlet and outlet boundary condition is also difficult for the DSMC method owing to its statistical nature.

In order to further validate the BGK–Burnett approach, we have calculated the mass flow rate through the channel for the pressure-driven Poiseuille flow. Both BGK–NS and BGK–Burnett schemes are used in the current calculation. The normalized mass flow rates are defined by $Q/\rho U^* h$, where Q is the mass flow rate and $\rho U^* h$ is the normalization factor. The velocity U^* is defined by $U^* = \alpha \sqrt{2kT/m}$, where α is related to the pressure gradient in the channel $p = p_0(1 + \alpha x/h)$ and h is the channel width. The calculated solutions, as well as the analytic solution of Ohwada, Sone & Aoki (1989), are shown in figure 8. From this figure, we can clearly see the improvement of the BGK–Burnett solution over the BGK–NS. For most microchannel flows in the laboratory, such as the experiments by Zohar *et al.* (2002), the highest Knudsen number at the outlet is about 0.2. Therefore, in the flow regime of these experiments, the slip Navier–Stokes equations are capable of capturing the physical solution. However, as the Knudsen number increases, such as up to 0.5, the

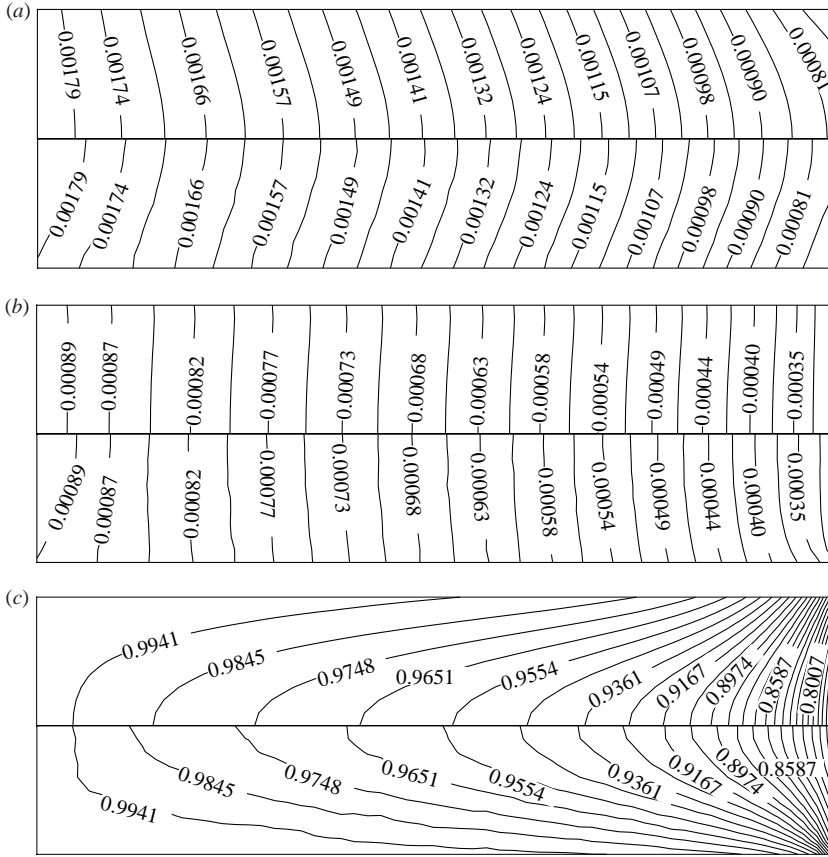


FIGURE 6. (a) Density, (b) pressure and (c) temperature contours for the pressure-driven Poiseuille flow with the domain $30l_0 \times 10l_0$, where l_0 is the mean free path. Upper part of the tube: BGK–Burnett; lower part of the tube: DSMC (Zheng *et al.* 2002b). In the temperature plot, non-dimensional contours T/T_{wall} are plotted.

BGK–Burnett should be a more appropriate numerical method than the Navier–Stokes ones.

3.2. Similarity pressure distribution along the microchannel

Based on the compressible Navier–Stokes equations and the slip boundary conditions, many authors have presented the analytic solutions for the microchannel flow. For example, Arkilic *et al.* (1997) presented a two-dimensional analysis with the first-order velocity slip boundary condition, and demonstrated the effects of both compressibility and rarefaction in long microchannels. They showed that the zero-order analytic solution corresponded well with the experimental results of Pong *et al.* (1994). Zohar *et al.* (2002) have solved the isothermal hydrodynamic equations using perturbation methods for both circular and planar microchannels. Their consistent expansions provide not only the cross-stream, but also the streamwise evolution of the various flow parameters of interest, such as pressure, density and Mach number. In terms of the pressure distribution, the difference between the results of Arkilic *et al.* (1997) and Zohar *et al.* (2002) are marginal. For example, the pressure distribution along

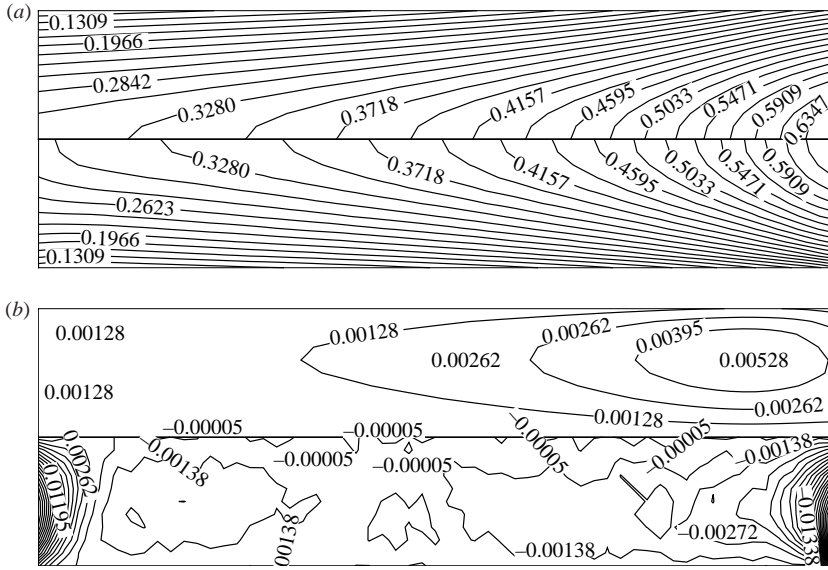


FIGURE 7. (a) U and (b) V velocity contours for the pressure-driven Poiseuille flow. Upper part of the tube: BGK–Burnett–lower part of the tube: DSMC (Zheng *et al.* 2002*b*).

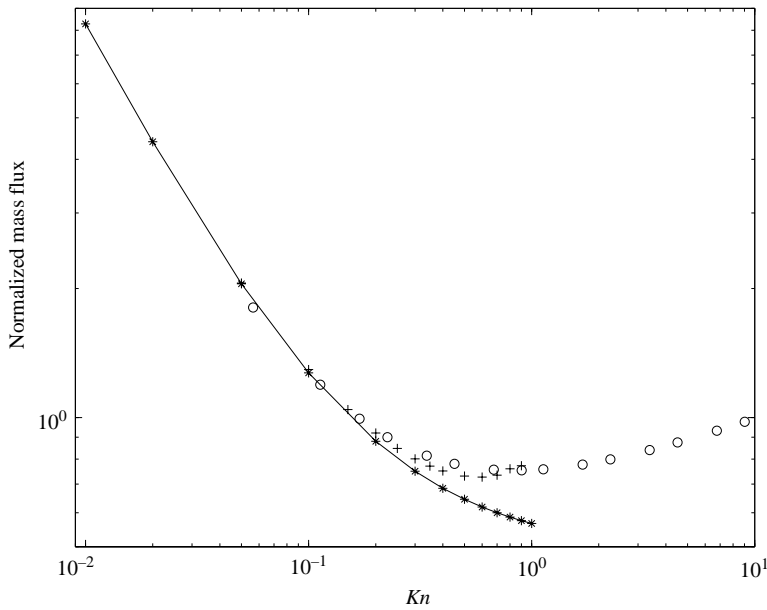


FIGURE 8. Relation of the normalized mass flow rate versus Knudsen number for the Poiseuille flow. \circ , solution of Ohwada *et al.* (1989); *—, BGK–NS (Xu 2001); +, gas-kinetic BGK–Burnett.

the central line of the channel can be simplified to the following similarity solution,

$$\frac{p(x)}{p_0} = -6Kn_0 + \left\{ \left(6Kn_0 + \frac{p_i}{p_0} \right)^2 - \left[\left(\frac{p_i^2}{p_0^2} - 1 \right) + 12Kn_0 \left(\frac{p_i}{p_0} - 1 \right) \right] \left(\frac{x}{L} \right) \right\}^{1/2}, \quad (21)$$

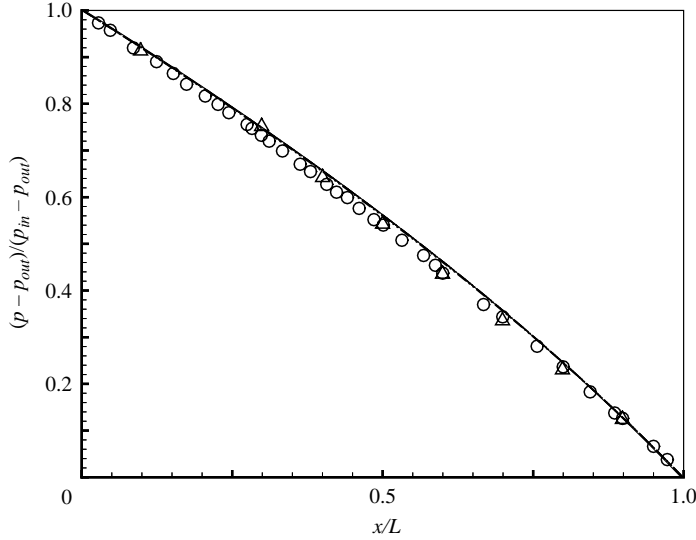


FIGURE 9. Solutions of pressure distribution along the microchannel for nitrogen gas with $H = 1.2 \mu\text{m}$ and $L = 36, 72, 108, 144, 216 \mu\text{m}$, respectively. The pressure ratio is $p_i/p_o = 1.891$. \circ , DSMC solution for $L = 36 \mu\text{m}$; Δ , experimental data of Pong *et al.* (1996), and all lines are the BGK–Burnett solutions with different channel lengths.

where L is the length of the channel, Kn_0 is the Kundsens number at the outlet, p_i and p_o are the pressures at the inlet and outlet separately, and x is the streamwise coordinates.

In order to test the validity of the similarity solution from the gas-kinetic BGK–Burnett method as well, we calculate a few cases with different channel lengths for the nitrogen gas. The channel and flow parameters are

$$H = 1.2 \mu\text{m}, \quad p_i/p_o = 1.891, \quad p_o = 101 \text{ kPa}, \quad T_w = 300 \text{ K},$$

and the total lengths are, respectively,

$$L = 36 \mu\text{m}, \quad 72 \mu\text{m}, \quad 108 \mu\text{m}, \quad 144 \mu\text{m}, \quad 216 \mu\text{m}.$$

The pressure distributions are shown in figure 9, as well as the DSMC results of Yan & Farouk (2002) for the short channel ($L = 36 \mu\text{m}$) and experimental data of Pong *et al.* (1994). As shown in this figure, there is a similarity pressure profile for the gas-kinetic BGK–Burnett solution, which is consistent with both the DSMC result and the experiment.

3.3. Pressure distribution and mass flow rate for long microchannels

In this subsection, we apply the gas-kinetic BGK–Burnett method to the study of subsonic long micro-channel flows. Zohar *et al.* (2002) obtained accurate measurements of the pressure distribution and mass flow rates for different gases, such as argon, helium and nitrogen, for a channel with $L = 4000 \mu\text{m}$. Since there is a similarity solution in pressure distribution, the solution (21) with zero flow velocity is used as the initial condition for the long microchannels. Then, the mass flow rate is evaluated after the steady-state solution is obtained.

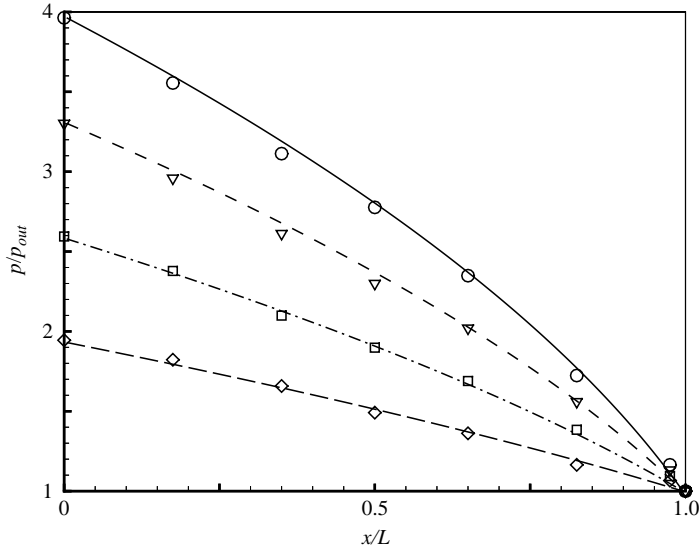


FIGURE 10. Pressure distributions for argon gas in a channel with $L = 4000 \mu\text{m}$ and $H = 0.53 \mu\text{m}$ for the pressure differences Δp (kPa) = 95.733, 161.533, 233.267, 300.267, respectively. Symbols, experimental data (Zohar *et al.* 2002); lines, BGK–Burnett solutions. —, cal. ($p_{in}/p_{out} = 3.963$; ---, 3.302; -·-, 2.594; ···, 1.945).

With the outlet pressure fixed as one standard atmosphere for the argon gas at room temperature, the experiments are carried out with the following pressure differences between the inlet and outlet,

$$\Delta P \text{ (kPa)} = 95.733, 161.533, 233.267, 300.267,$$

and the corresponding pressure ratios are

$$p_{in}/p_{out} = 1.945, 2.594, 3.302, 3.963.$$

The measured pressure profiles along the channel as well as the simulation results from the BGK–Burnett method are shown in figure 10. In order to see the nonlinearity in the pressure distribution, the deviation between the pressure distribution and the linear one, i.e. $(p - p_{linear})/p_o$, is plotted in figure 11 for both cases of ΔP (kPa) = 161.533 and 300.267. The analytic solutions based on (21) are also included. From this figure, we can clearly see that both the direct BGK–Burnett solution and the analytic solution of the Navier–Stokes equations have stronger nonlinearity than the experimental results for the high pressure ratio case, and the analytic solutions for the NS equations are slightly shifted to the downstream region. For the nitrogen gas with pressure differences

$$\Delta \text{ (kPa)} = 241.5068, 179.6701, 112.3367,$$

the measured pressure distributions and the BGK–Burnett solutions are shown in figure 12. The nonlinear deviation $(p - p_{linear})/p_o$ from the experiments, BGK–Burnett solutions, and the analytic one (21), are presented in figure 13. Different from the monatomic argon gas, the nonlinearity of the BGK–Burnett solution for the diatomic nitrogen is stronger than the analytic one. As tested by varying the viscosity coefficient,

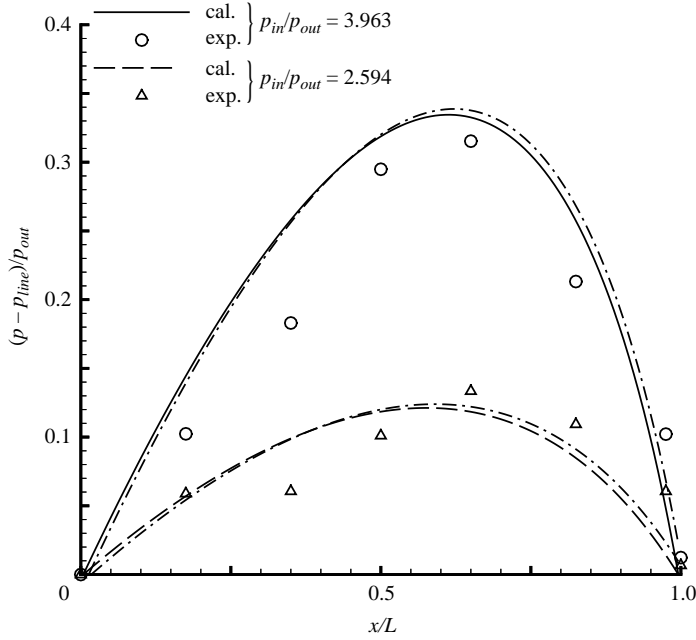


FIGURE 11. The deviation from the linear pressure distribution for argon gas with $p_i/p_o = 3.963, 2.594$. Symbols, experimental results (Zohar *et al.* 2002). —, ---, BGK–Burnett. -.-, analytic solution of the Navier–Stokes solutions (Arklic *et al.* 1997).

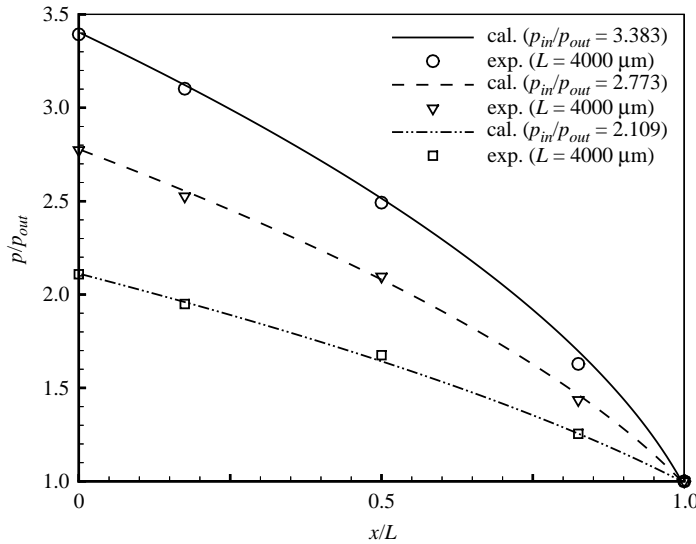


FIGURE 12. Pressure distributions for nitrogen gas in a channel with $H = 0.97 \mu\text{m}$ and $L = 4000 \mu\text{m}$ for the pressure differences Δp (kPa) = 241.5068, 179.6701, 112.3367. Symbols, experiments (Zohar *et al.* 2002); lines, BGK–Burnett.

the deviation is not caused by the additional bulk viscosity contribution in the BGK–Burnett solution, it results mainly from the extra term in the Burnett equations in comparison with the Navier–Stokes equations.

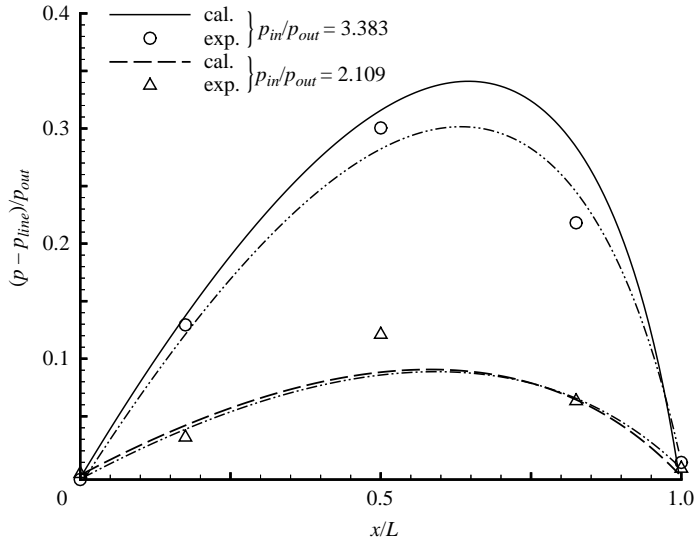


FIGURE 13. The deviation of the pressure from the linear distribution for nitrogen gas. \circ , experiments for $p_i/p_o = 3.383$ and $p_i/p_o = 2.109$ (Zohar *et al.* 2002). —, ---, BGK–Burnett. \cdots —, analytic Navier–Stokes solution (Arkilic *et al.* 1997).

In terms of the mass flow rates, Zohar *et al.* (2002) have tested the argon, nitrogen, and helium gases with the following pressure differences

$$\text{argon : } \Delta P \text{ (kPa)} = 100.60, 167.50, 234.20, 299.93, 365.90,$$

$$\text{nitrogen : } \Delta P \text{ (kPa)} = 101.73, 169.43, 236.43, 301.47, 368.10,$$

$$\text{helium : } \Delta P \text{ (kPa)} = 102.10, 169.40, 234.50, 302.10, 366.27.$$

The microchannels have the heights $H = 0.53 \mu\text{m}$ and $0.97 \mu\text{m}$, respectively, with the length $L = 4000 \mu\text{m}$. The calculated mass flow rates based on the BGK–Burnett method for different gases in the case of $H = 0.53 \mu\text{m}$ are shown in figure 14. The differences between the calculations and experiments are of the order of 2% – 10%. Figure 15 shows the results for the nitrogen gas for a channel with $H = 0.97 \mu\text{m}$ and $H = 0.53 \mu\text{m}$, respectively. For the $H = 0.53 \mu\text{m}$, the results for nitrogen gas are the same as those in figure 14. The pressure differences for the $H = 0.97 \mu\text{m}$ case are

$$\Delta P \text{ (kPa)} = 101.0, 127.0, 163.0, 193.0, 233.5, 300.0, 365.0,$$

which give the pressure ratios

$$p_{in}/p_{out} = 1.997, 2.253, 2.609, 2.905, 3.304, 3.961, 4.602.$$

Figure 15 shows that the simulation results take a smooth curve between the pressure difference and the mass flow rate in comparison with the experimental one. There seems to be a slight jump in the experimental mass flow rate around $\Delta p = 200 \text{ kPa}$. As demonstrated in Zohar *et al.* (2002) and many others, only the compressibility and slip-flow effects are important for the mass flow rate, where the flow acceleration and the non-parabolic velocity profile can be neglected. In all calculations, we found that the calculated mass flow rates are slightly lower than the experimental ones. This is probably due to the use of a fully diffuse reflection boundary. As shown by

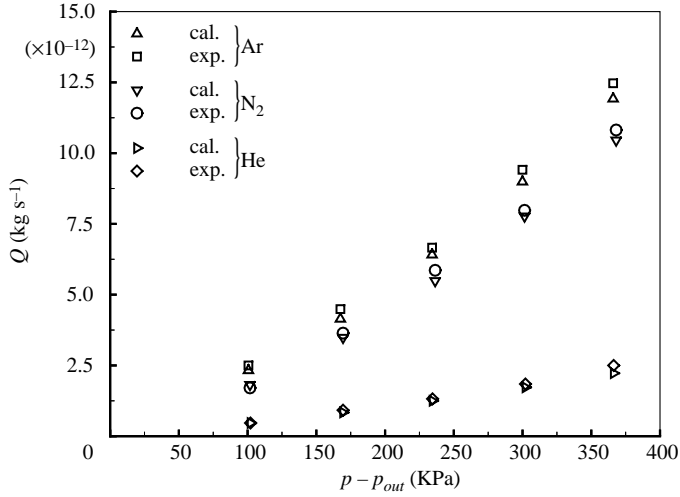


FIGURE 14. Mass flow rates for argon, nitrogen and helium for the channel with $H = 0.53 \mu\text{m}$ and $L = 4000 \mu\text{m}$. The simulation results are slightly lower than the experimental ones owing to the use of the full accommodation boundary condition.

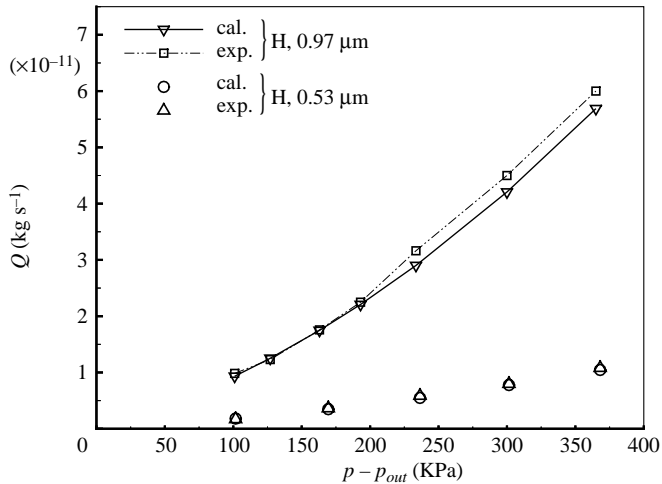


FIGURE 15. Mass flux rates for nitrogen with $H = 0.97 \mu\text{m}$ and $0.53 \mu\text{m}$.

Arkilic *et al.* (2001), the gas may not be fully accommodated at the boundary, and the mass flow rate will increase subsequently when the value σ is less than 1.

4. Conclusion

In this paper, we first construct a gas-kinetic BGK–Burnett scheme based on the gas-kinetic BGK model and second-order expansions for the Maxwell–Boltzmann distribution function. Then, the scheme is applied to study the microchannel flow in the slip flow regime. For the Poiseuille flow at $Kn=0.1$, it is found that the BGK–Burnett scheme gives a more accurate solution than the schemes based on the Navier–Stokes equations with slip boundary condition. In other words, if a detailed

solution is required in the cross-stream direction in the slip flow regime, equations higher than the Navier–Stokes order, such as the Burnett, are needed. However, in the streamwise direction at $Kn = 0.1$, the difference between the solutions from the Navier–Stokes and BGK–Burnett are small. Since in the near continuum flow regime, both DSMC and the direct solver of the Boltzmann equation have great difficulties in terms of their accuracy because of the statistical noise, inlet and outlet boundary conditions, and the decoupling between the collision and transport process, the gas-kinetic schemes based on the continuum model in the particle velocity space may play an important role here. In the second part of this paper, we use the gas-kinetic BGK–Burnett scheme to study long microchannel flows, where the simulation results match the experimental measurements accurately. Therefore, we can use the BGK–Burnett solver in the study of flow phenomena in slip flow regime in the microchannels. However, for the shock-wave calculation, it seems impossible to use the current BGK–Burnett method to give an accurate solution in the high-Mach-number case, such as $M \geq 3.0$ (Xu 2002). From our experience, we believe, like many others, that in the shock-wave calculations, the Burnett type equations could work properly and accurately only in cases where the Navier–Stokes equations do not fail and higher-order equations could provide more accurate solutions. However, for the channel flow, as shown in figure 8, the current BGK–Burnett method gives a more accurate and reliable solution than the BGK–NS in the flow regime $Kn \leq 1.0$. In the future, the BGK–Burnett scheme will be further used in the studies of the near continuum and continuum flow phenomena, such as the ghost effects (Sone 2000) in terms of the Navier–Stokes equations.

K. X. would like to thank Professor Ohwada for helpful discussion about the Chapman–Enskog expansion, Professor Zohar for providing the experimental data, and Mr M. L. Mao for his help in calculating the data in figure 8. We would like to thank all reviewers for their constructive comments and suggestions, which greatly improved the quality of the manuscript. This work was supported by Hong Kong Research Grant Council.

REFERENCES

- AGARWAL, R. K., YUN, K. Y. & BALAKRISHNAN, R. 2001 Beyond Navier–Stokes equations for flows in the continuum-transition regime. *Phys. Fluids* **10**, 3061–3085.
- AOKI, K., TAKATA, S. & NAKANISHI, T. 2002 Poiseuille-type flow of a rarefied gas between two parallel plates driven by a uniform external force. *Phys. Rev. E* **65**, 026315:1.
- ARISTOV, V. V. 2001 Direct methods for solving the Boltzmann equations and study of non-equilibrium flows, Kluwer.
- ARKILIC, E. B., BREUER, K. S. & SCHMIDT, M. A. 2001 Mass flow and tangential momentum accommodation in silicon micromachined channels. *J. Fluid Mech.* **437**, 29–43.
- ARKILIC, E. B., SCHMIDT, M. A. & BREUER, K. S. 1997 Gaseous slip flow in long microchannels. *J. Microelectromech. Syst.* **6**, 167–178.
- BALAKRISHNAN, R. 1999 Entropy consistent formulation and numerical simulation of the BGK–Burnett equations for hypersonic flows in the continuum-transition regime, PhD thesis, Wichita State University.
- BESKOK, A. & KARNIADAKIS, G. E. 1999 A model for flows in channels, pipes, and ducts at micro and nano scales. *Microscale Thermophys. Engng* **3**, 43–77.
- BHATNAGAR, P. L., GROSS, E. P. & KROOK, M. 1954 A model for collision processes in gases I: Small amplitude processes in charged and neutral one-component systems. *Phys. Rev.* **94**, 511–525.
- BIRD, G. 1994 *Molecular Gas Dynamics and the Direct Simulation of Gas Flows*. Clarendon.

- CAI, C., BOYD, D., FAN, J. & CANDLER, G. V. 2000 Direct simulation methods for low-speed microchannel flows. *J. Thermophys. Heat Transfer* **14**, 368–378.
- CERCIGNANI, C. 2000 *Rarefied Gas Dynamics*. Cambridge University Press.
- CHAE, D., KIM, C. & RHO, O. H. 2000 Development of an improved gas-kinetic BGK scheme for inviscid and viscous flows. *J. Comput. Phys.* **158**, 1.
- FAN, J. & SHEN, C. 2001 Statistical simulation of low-speed rarefied gas flows. *J. Comput. Phys.* **167**, 393–412.
- HO, C. M. & TAI, Y. C. 1998 Micro-Electro-Mechanical-Systems (MEMS) and Fluid Flows, *Annu. Rev. Fluid Mech.* **30**, 579.
- KARNIADAKIS, G. E. & BESKOK, A. 2002 *Microflows: Fundamentals and Simulation*. Springer.
- LI, Z. H. & ZHANG, H. X. 2004 Study on gas kinetic unified algorithm for flows from rarefied to continuum. *J. Comput. Phys.* **193**, 708–738.
- MALEK, M. M., BARAS, F. & GARCIA, A. L. 1997 On the validity of hydrodynamics in plane Poiseuille flows. *Physica A* **240**, 255.
- OHWADA, T. 2002 On the construction of kinetic schemes. *J. Comput. Phys.* **177**, 156–175.
- OHWADA, T. & KOBAYASHI, S. 2004 Management of the discontinuous reconstruction in kinetic schemes. *J. Comput. Phys.* **197**, 116–138.
- OHWADA, T., SONE, Y. & AOKI, K. 1989 Numerical analysis of the Poiseuille flow and thermal transpiration flows between two parallel plates on the basis of the linearized Boltzmann equation for hard-sphere molecules. *Phys. Fluids* **1**, 2042.
- OHWADA, T. & XU, K. 2003 The kinetic scheme for the full-Burnett equations. *J. Comput. Phys.* (submitted).
- ORAN, E. S., OH, C. K. & CYBYK, B. Z. 1998 Direct simulation Monte Carlo: recent advances and applications. *Annu. Rev. Fluid Mech.* **30**, 403–441.
- PATTERSON, G. N. 1956 *Molecular Flow of Gases*. Wiley.
- PIEKOS, E. S. & BREUER, K. S. 1996 Numerical modeling of micromechanical devices using the direct simulation Monte Carlo method. *Trans. ASME I: J. Fluids Engng* **118**, 464–469.
- PONG, K. C., HO, C. M., LIU, J. Q. *et al.* 1994 Nonlinear pressure distribution in uniform microchannels. *ASME-FED* **197**, 51–56.
- SANTOS, A., BREY, J. J., KIM, C. S. & DUFTY, J. W. 1989 Velocity distribution for a gas with steady heat flow. *Phys. Rev. A* **39**, 320.
- SHAKHOV, E. M. 1968 Generalization of the Krook kinetic relaxation equation. *Fluid Dyn.* **3**, 95.
- SONE, Y. 2000 Flows induced by temperature fields in a rarefied gas and their ghost effect on the behavior of a gas in the continuum limit. *Annu. Rev. Fluid Mech.* **32**, 779–811.
- URIBE, F. J. & GARCIA, A. L. 1999 Burnett description for plane Poiseuille flow. *Phys. Rev. E* **60**, 4063–4078.
- VINCENTI, W. G. & KRUGER, JR. C. H. 1965 *Introduction to Physical Gas Dynamics*. Wiley.
- XU, K. 2001 A gas-kinetic BGK scheme for the Navier–Stokes equations and its connection with artificial dissipation and Godunov method. *J. Comput. Phys.* **171**, 289–335.
- XU, K. 2002 Regularization of the Chapman–Enskog expansion and its description of shock structure. *Phys. Fluids* **14**, L17.
- XU, K. 2003 Super-Burnett solutions of Poiseuille flow. *Phys. Fluids* **15**, 2077.
- YAN, F. & FAROUK, B. 2002 Numerical simulation of gas flow and mixing in a microchannel using the direct simulation Monte Carlo method. *Microscale Thermophys. Engng* **6**, 235–251.
- ZHENG, Y., GARCIA, A. L. & ALDER, B. J. 2002a Comparison of kinetic theory and hydrodynamics for Poiseuille flow. *J. Stat. Phys.* **109**, 495–505.
- ZHENG, Y., GARCIA, A. L. & ALDER, B. J. 2002b Comparison of kinetic theory and hydrodynamics for Poiseuille flow. *Rarefied Gas Dynamics*, vol. 23, Whistler, Canada.
- ZOHAR, Y., LEE, S. Y. K., LEE, W. Y., JIANG, L. & TONG, P. 2002 Subsonic gas flow in a straight and uniform microchannel. *J. Fluid Mech.* **472**, 125–151.